Mathematical investigation of tsunami-like long waves interaction with submerge dike of different thickness

Konstantin Zhiltsov, Kirill Kostyushin, Anuar Kagenov, and Ilya Tyryshkin

Citation: AIP Conference Proceedings **1899**, 060006 (2017);
View online: https://doi.org/10.1063/1.5009877
View Table of Contents: http://aip.scitation.org/toc/apc/1899/1
Published by the American Institute of Physics

Mathematical Investigation of Tsunami-like Long Waves Interaction with Submerge Dike of Different Thickness

Konstantin Zhiltsov[a)], Kirill Kostyushin, Anuar Kagenov and Ilya Tyryshkin

Research Institute of Applied Mathematics and Mechanics of Tomsk State University, 36 Lenina Avenue, Tomsk 634050, Russia

[a)]Corresponding author: konstantin@niipmm.tsu.ru

Abstract. This paper presents a mathematical investigation of the interaction of a long tsunami-type wave with a submerge dike. The calculations were performed by using the freeware package OpenFOAM. Unsteady two-dimensional Navier-Stokes equations were used for mathematical modeling of incompressible two-phase medium. The Volume of Fluid (VOF) method is used to capture the free surface of a liquid. The effects caused by long wave of defined amplitude motion through a submerged dike of varying thickness were discussed in detail. Numerical results show that after wave passing through the barrier, multiple vortex structures were formed behind. Intensity of vortex depended on the size of the barrier. The effectiveness of the submerge barrier was estimated by evaluating the wave reflection and transmission coefficients using the energy integral method. Then, the curves of the dependences of the reflection and transmission coefficients were obtained for the interaction of waves with the dike. Finally, it was confirmed that the energy of the wave could be reduced by more than 50% when it passed through the barrier.

INTRODUCTION

Tsunami wave is one of the most destructive natural phenomena. Tsunamis are especially dangerous in coastal regions. Generating in the ocean a long tsunami wave reaches a shoreline and destroying everything in its path. Inability to detect tsunami wave in the open seas and a sharp increase of the amplitude after reaching the coastline makes the tsunami wave unpredictable and dangerous phenomenon [1].

Most scientific research of tsunami problems are carried out jointly with experiment. It is worth noting some fundamental work in the field of tsunami research. Losada et al. in [2] studied the results of solitary wave interaction with a ledge, Friedman et al in [3] conducted experiments of the wave interaction with several impermeable submerge barriers. Experimental works by Irtem et al. [4], Saprykina et al. [5], were devoted to a wave interaction with a permeable and impenetrable obstacle with different amplitude of waves. It is important to note the work of Sriram et al. [6] which was conducted in a large wave channel in Germany (GWK). In our works [7, 8], the method of experimental investigation of tsunami waves in a hydrodynamic facility is detailed, and there is a patent certificate [9]. However, conducting an experiment always extremely costly way. That is why an important place occupied by analytical and numerical methods.

In our time, a number of mathematical approaches are using to calculate nonlinear long waves. The model of the nonlinear theory of shallow water is widely used based on the Boussinesq, Korteweg-de-Fries, and Euler equations [2, 6, 10, 11]. At the same time, such models, for the most part, do not take viscosity into account, which is critical in the evaluation of vortices. Another direction is relating to the solution of the Navier-Stokes equations for a viscous incompressible fluid [12, 13]. For example, Wijatmiko et al. [14] and Jesus et al. [15] used the Navier-Stokes equations to study the process of passage of a long solitary wave through porous and impenetrable [15] obstacles.

In papers [16, 17] describe a solitary wave passing through a submerge barrier of finite length. The generation process of vortex structures above and after the barrier is considered. Velocity profiles in the two-dimensional coordinate system are estimate. Interesting is the work [18] in which the Lagrangian method of the Smoothed Particles Hydrodynamics is used as a computational method. It is especially important to consider the work of Qu et al. [19], in which the popular practice of calculating a solitary wave is refute. It notes that the calculation of a solitary wave leads to an underestimation of the total energy and to incorrect evaluation of the

Prospects of Fundamental Sciences Development (PFSD-2017)
AIP Conf. Proc. 1899, 060006-1–060006-10; https://doi.org/10.1063/1.5009877
Published by AIP Publishing. 978-0-7354-1587-4/$30.00

run-up. Jiang et al. [20] investigated the interaction of a solitary tsunami wave with a vertical wall. The calculations were carried out in a three-dimensional condition using the OpenFOAM package.

The authors of this paper have already completed some studies of tsunami problems. In paper [21] the comparison results of the experiment and mathematical modeling were presented for the first time. The analysis has shown that the evaluation of long waves relative to the amplitude and depth of the channel bring a result in a very narrow range, when $A/H \leq 0.1$. In [22] for the first time was proposed the dimensionless parameter $h/(H+A)$, taking into account not only the height of the wave but also the height of the barrier. Within this parameter, the amplitude coefficient of long wave reflection is describe by the dependence in a wider range of $A/H \leq 0.3$. The results for the sum of the relative energies of the reflected and transmitted waves has shown that the maximum efficiency was achieved when $h/(H+A) \approx 0.8 – 0.95$ and the energy of the transmitted wave was reduced by 50%. In [23] for the first time the results of mathematical calculations for a complex of two barriers were presented. The results of paper [23] showed that when the distance between the barriers is $2H$, the maximum extinction of the transmitted wave takes place. This effect is due to the formation of vortex structures behind the barriers. Data obtained in [23] were compared with the results of [3] and showed good qualitative agreement.

In this paper, we continue to study the interaction of long waves with impermeable dikes using numerical simulation of a viscous fluid based on the two-dimensional Navier-Stokes equations. We show a detailed investigation of the wave propagation through the barriers of the different thicknesses in order to estimate the process of generation and evolution of vortex structures beyond the barrier. The integral method of calculating the transmitted and reflected wave energy was used to determine the effectiveness of the impermeable barriers.

EXPERIMENT SETUP

Experimental studies were carried out in a Big Hydrodynamic Channel (BHC) in Institute of Applied Mechanics of Russian Academy of Sciences of the Russian Academy of Sciences. Channel dimensions: length – 15 m, width – 0.26 m, height – 0.4m. Most methods of wave generation were performed using movable elements. There are no moving parts in our hydrodynamic channel. Method of gravitational waves initiation is based on the breakdown of an arbitrary discontinuity of water levels in the channel. At the beginning of the channel there was a generator compartment with a length of $a = 1.5$ meters. From the main cavity generator is separated by a bridge. Then the air is evacuated via tube from the upper part of the generator thereby attaining specified water level difference ξ_0: depth in generator $(H+\xi_0)$, depth in work part of the channel is H. After depressurization of the upper part of the generator, in the working part of the channel the wave is initiated with length $\lambda = 2a$ and amplitude $A = \xi_0/2$. More detailed information about the experimental conditions and comparison with numerical calculations can be found in our works [7, 8, 21, 22].

NUMERICAL MODEL

Government Equations

A schematic diagram of a wave passing over a rectangular dike is shown in Fig. 1. Channel depth H, barrier thickness D, barrier height h, wave amplitude A.

For the problem of a viscous incompressible fluid motion, the system of Navier-Stokes equations solved in a two-dimensional formulation. In vector form, the system includes the continuity equation:

$$\nabla \mathbf{U} = 0; \tag{1}$$

equation of motion:

$$\rho \frac{\partial \mathbf{U}}{\partial t} + \nabla(\rho \mathbf{U}\mathbf{U}) = -\nabla p + \eta \nabla^2 \mathbf{U} + \rho g - \sigma_T k_\gamma \nabla \gamma \tag{2}$$

where $\mathbf{U} = (u, v)$ is the velocity vector of the mean flow, $\nabla - (\partial/\partial x, \partial/\partial y)$, ρ is fluid density, p is the pressure in excess of the hydrostatic, g is the gravitational acceleration vector ($g = 9{,}81$ m/s). The last term of Eq. (2) is the effect of surface tension, in which the σ_T is the surface tension coefficient 0.0728 kg/s^2, γ is a scale field used to track the fluid, $k_\gamma = \nabla\left(\nabla\gamma / |\nabla\gamma|\right) = \nabla n$ is the surface curvature.

The free surface between water and air is captured using the volume of fluid method (VOF), which was originally proposed by Hirt and Nichols [24]. The transportation equation of volume of fluid has the following form:

$$\frac{\partial \gamma}{\partial t} + \nabla(\gamma \mathbf{U}) = 0 \tag{3}$$

where γ is the volume fraction was defined by whether the control volume is filled by water or air, as:

$$\gamma = \begin{cases} \gamma = 0, \ air \\ 0 < \gamma < 1, \ interface \\ \gamma = 1, \ water \end{cases} \tag{4}$$

The local density and laminar viscosity as functions of γ are compute as:

$$\begin{aligned} \rho &= \gamma \rho_{water} + (1-\gamma)\rho_{air} \\ \eta &= \gamma \eta_{water} + (1-\gamma)\eta_{air} \end{aligned} \tag{5}$$

In our work we solve the problem without taking turbulence into account. We believe that this approach is justified, since in our case the critical number Re^* does not exceed 10^4. It is known from experiments in rectangular channels [25] that Reynolds numbers of transition to the turbulent state is high enough 10^4 (at $x/H = 60$ transition Reynolds number is $1.8 \cdot 10^4$). Moreover, as the initial perturbations decrease, the critical Reynolds number increases even more. In our case $\lambda = 3$ m, $H \approx 0.1$ m ($x/H \leq 30$) and the initial perturbations before the wave are zero.

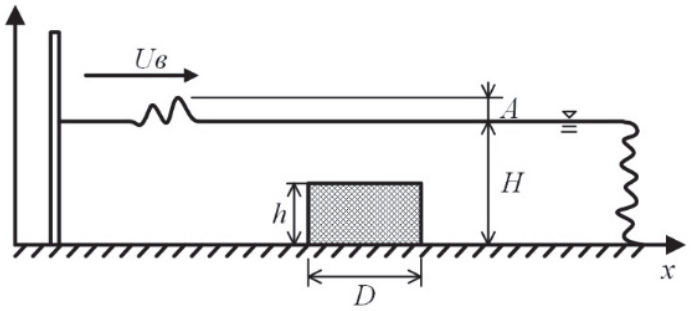

FIGURE 1. Schematic diagram of a wave passing over a submerged dike

Initial and Boundary Conditions

The boundary conditions on the rigid walls of the channel (and the walls of the rigid obstacle) are set as follows:

$$\mathbf{U} = 0 \tag{6}$$

The conditions at the upper boundary of the computational area are set in accordance with the method of computational algorithm of OpenFOAM package:

$$n \cdot \mathbf{U} = 0 \tag{7}$$

$$p_{atm} = 1 \ \text{atm.} \tag{8}$$

At the initial time given the distribution of the volume concentration γ, corresponding to the initial state of the water level in the channel and the generator. With the beginning of calculation under the influence of gravity wave motion begins. Conditions for the distribution of velocity and pressure at $t = 0$ were set equal to zero.

In Wu et al. [16] and Jiang et al. [20], in connection with the peculiarity of a solitary wave formation, it was necessary to get rid of the reflected waves in the channel. For this, the left border was completely absorbing. In the case of our wave generating method, such a need arises. In addition, it is not possible to specify exactly the conditions for the absorption of a wave at a far boundary when the flow height $H + \xi$ is unknown. In this case, we simply extend the computational domain long enough such that the wave does not reach the downstream boundary of the domain.

Experiments Conditions and Investigation Methods

In this paper presents the results of propagation and interaction of a long gravitational wave with an impermeable submerge dike of various thicknesses. Numerical calculations were carried out with the value of the dimensionless parameter $h/(H+A) \approx 0.864$. Consequently, the height of the dike for all cases $h = 0.095$ m, depth of calm water $H = 0.103$ m and amplitude of the wave $A = 0.007$ m (parameter $A/H = 0.068$). Thus, the results of calculations far from the dike can be well described by the linear theory [21].

Conventionally, the effectiveness of the dike is estimated in terms of the wave reflection and transmission coefficients. They are usually based on linear wave theory, which assumes that the flow irrotational and solely

dependent on wave height. For non-linear waves, the energy integral method, based on the integration of energy flux, is more appropriate.

In the linear theory of shallow water, the equality of the potential and kinetic energy is suppose. Therefore, to calculate the total energy of a wave is often use this assumption, and calculating the total energy as doubled potential energy by the following integral formula:

$$W_{pot} = \rho g \int_0^{\lambda} \xi^2 dx = \rho g \sqrt{gH} \int_0^{t} \xi^2 dt \tag{9}$$

In the left part of Eq. (9), the wave energy was calculated through the spatial integral. It is usually more convenient to use the time integral on the right part of Eq. (9).

Numerical Setup

The mathematical model described above with initial and boundary conditions was solved by a finite volume method [26]. The numerical calculation was carried out on an Eulerian grid, which means that the shape and size of the computational cells are fixed. The length of the computational domain varied from 15 m to 30 m, height and width were constant: 0.13 m and 0.02 m, respectively. According to the *x*-axis grid spacing remains constant 0.002 m. On the *y*-axis, the grid spacing was varied from 0.001 m to 0.002 m. The computational grid along *y*-axis was condensed in a small region at the water-air interface to obtain more accurate of calculations. The *z*-axis had only one calculated cell. The necessity to specify the dummy *z*-axis in the two-dimensional problem is cause by the peculiarity of the OpenFOAM software package. Example of the calculated grid with the dike can be seen in Fig. 2.

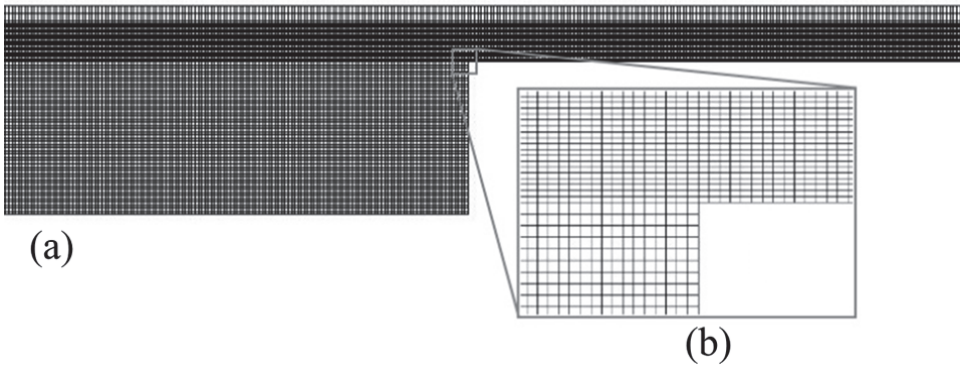

FIGURE 2. (a) Computational grids in the numerical domain, (b) refined grids around the obstacle

The time step was non-fixed and was calculated automatically by an explicit scheme of the first order of accuracy from the condition that the Courant number should not exceed 0.6. Calculation of a wave passing through the channel took from 20 to 45 s and was interrupted when the incident wave reached the right wall of the channel. The recording of the calculation data was carried out every 0.01 s.

The calculations were performed using the OpenFOAM package [27]. Open GNU-licensed OpenFOAM package is a set of open source libraries and macroses written in C++, and, in fact, is a sort of programming language and a handy tool for numerical simulation of physical processes in the continuum mechanics.

RESULTS AND DISCUSSION

Wave Generation and Evolution Process

Figure 3 shows the results of numerical and experimental investigation of wave process in BHC during initiation of tsunami wave by the ideal generator. At $t = 0$ (Fig. 3,a) there is the initial distribution of water levels in the wave generator ($x < 1.5$ m) and the channel. At the bottom (below the white horizontal line), the scale of longitudinal velocity U is shown. We can see that at $t = 0$ the velocities in wave generator and channel are equal to zero. At $t = 0.5$ sec (Fig. 3,b) and $t = 1.5$ sec (Fig. 3,c) we can see two waves that propagate in the different directions. Further, at $t = 3$ sec (Fig. 3,d) we see the reflection of the wave, which propagated to the left, from the rear wall ($x = 0$ m) of the generator. At the time $t = 4.5$ sec (Fig. 3,e) the shaping of gravitational

wave is almost completed. At this moment, the fluid velocities before the wave are zero, after the wave small oscillations was observed, which are also close to zero.

Figure 4 shows a comparison of experimental oscillogram of wave height versus time $\xi(t)$ with calculated dependence for ideal generator [28]. The numerical profile of the wave was obtained at a distance $x = 5.245$ m from the beginning of the channel (or $x = 3.745$ m from the front wall of the generator). At the same distance, an experimental wave profile was also obtained from the sensor No. 1 installed in the BHC. As can see, the numerical profile quite accurately coincides with the wave profile obtained in the experiment. The arrival time of the wave on the sensor and the height of the shear of the free surface $\xi(t)$ both coincide. Nevertheless, it is worth noting that the experimental sensors react more strongly to the displacement of the wave profile. This explains the significant number of small oscillations, which are usually smoothed in numerical simulation.

Figure 5 shows the time waveform of the free surface of water displacement as a result of a wave passing for the case when the thickness of the dike is $D = 0.01$ m. Sensor No. 1, located at a distance $x = 5.245$ m from the beginning of the channel, detects the incident and reflected waves. Sensor No. 2, located at a distance $x = 11.2$ m from the beginning of the channel, detects the wave transmitted through the dike, the front edge of which is set at a distance $x = 9.04$ m. Data records similar to the Fig. 5 were recorded for all numerical calculations for different thicknesses of the dike D.

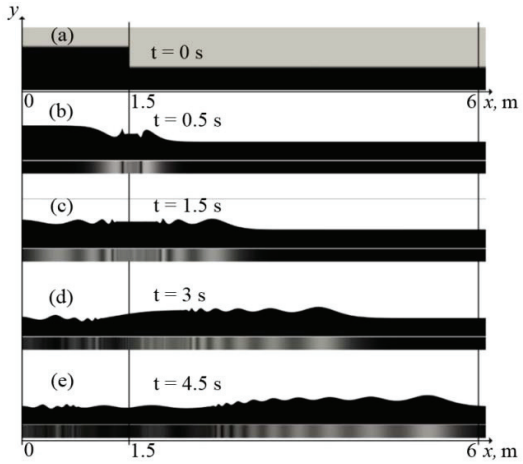

FIGURE 3. Numerical simulation of tsunami-kind wave shaping process by the ideal generator at $H = 0.103$ m, $A = 0.007$ m

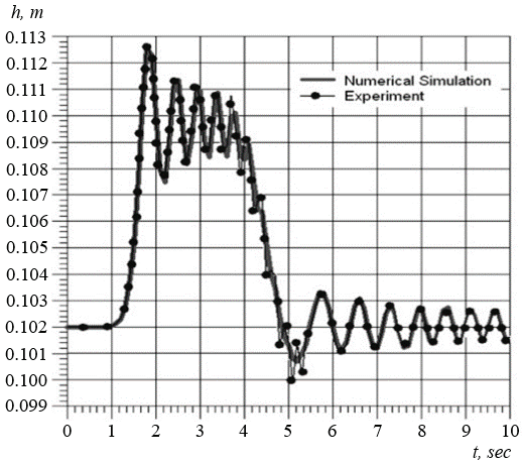

FIGURE 4. Comparison of experimental dependence wave height – time $\xi(t)$ with the numerical calculation for ideal generator at a distance of $x = 5.245$ m from the beginning of the channel

Figure 6 shows the velocity magnitude vectors for two characteristic cases of interaction at time t =7-8.5 sec. On the right in the Fig. 6 (b, d, f) the barrier with thickness $D = 6$ m (which is twice the wavelength $\lambda = 3$ m), on the left the barrier with thickness $D = 0.01$ m (Fig. 6 a, c, e). As can be seen, with the wave run-up on a short obstacle, the formation of vortices occurs with low intensity. In the case of a long obstacle, when each crest run-

up over a barrier, generation of vortex structures of a longer length occurs in the near-wall region. The length of all formed vortices is twice the thickness of the short barrier. Thus, on a short obstacle the vortex does not have time to form. As can be seen from Fig. 5, the wave consists of several ridges. When the wave run-up on a barrier with thickness $D = 6$ m (Fig. 6,b; 6,d; 6,e) the rolling of each ridge cause the formation of a vortex on the near-wall region. This effect can cause an additional reduction in the strength of the wave. It is worth paying attention to an interesting fact, at the same moments of time the speed over the short obstacle differs in the big direction in comparison with the long obstacle.

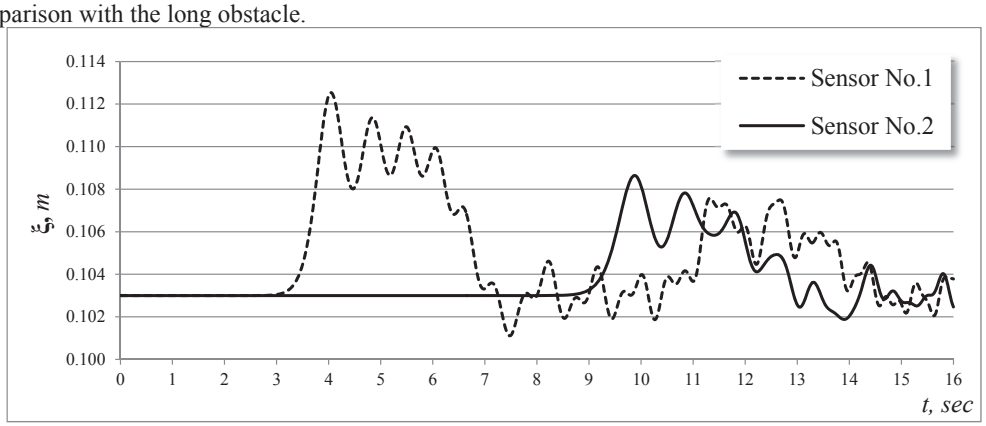

FIGURE 5. The profiles of the free surface motion as a function of time at distances $x = 5.245$ m (sensor No.1) and $x = 11.2$ m (sensor No.2) at $H = 0.103$ m, $A = 0.007$ m, $D = 0.01$ m

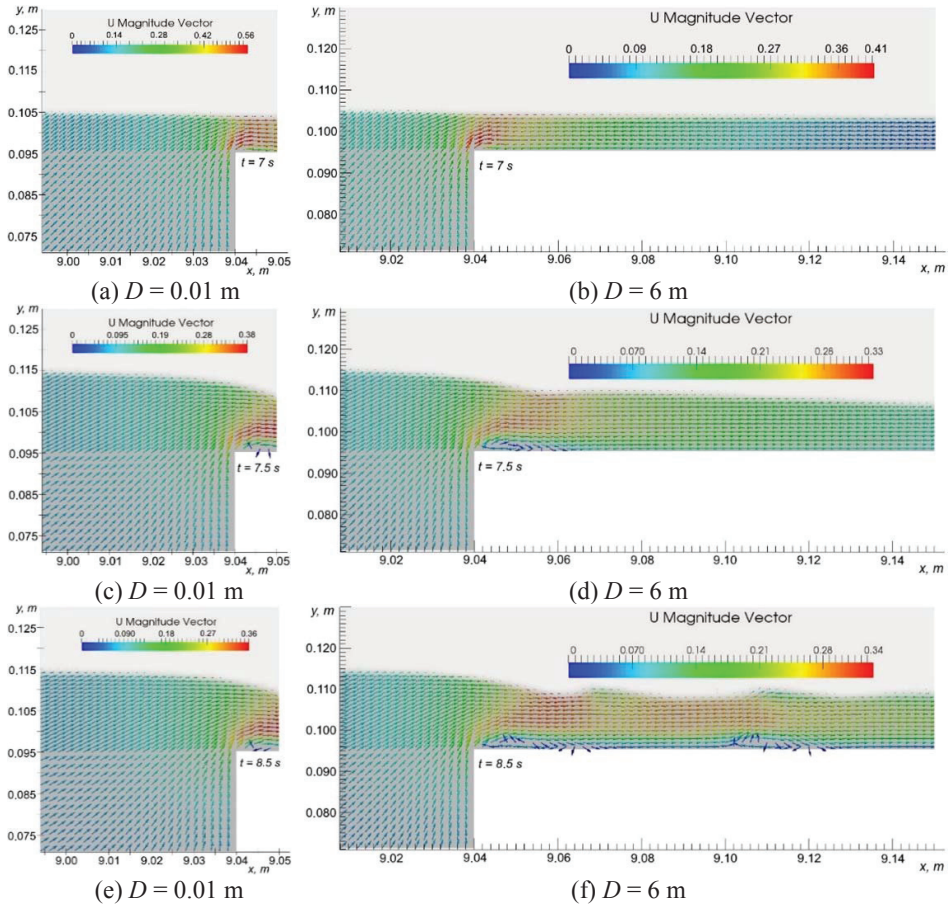

(a) $D = 0.01$ m (b) $D = 6$ m

(c) $D = 0.01$ m (d) $D = 6$ m

(e) $D = 0.01$ m (f) $D = 6$ m

FIGURE 6. Pictures of the distribution of velocity vectors at different times for a thin barrier $D = 0.01$ m (a, c, e) in comparison with a thick barrier $D = 6$ m (b, d, f)

In our study, the power of extinction of the wave energy which passing through the barrier is the key factor. We do not take into account the force of pressure on the obstacle and, therefore, the evolution of the flow behind the barrier is of most interest. Figure 7 shows the evolution of the flow behind a thin obstacle in dimensional coordinates, when $D = 0.01$ m. When the wave flows through a barrier, one large vortex immediately forms. Over time, several small perturbations arise on large vortex boundaries, which rotate in the opposite direction. At times when the wave has already passed through the barrier and is at a distance greater than the wavelength λ (Fig. 8, $t = 14$ sec, $t = 16$ sec) the flow is stabilized and clear vortex structures of different intensity can be seen. The strongest vortex is still near the obstacle.

Figure 8 presents analogous velocity distributions at different instants of time for a barrier of thickness $D = 6$ m. The maximum velocity distribution is concentrated long enough in the surface layer. This effect is explained by the thickness of the barrier – it is much longer than the wavelength. Thus, passing over the obstacle the wave become slowed and longest. A similar effect of wave deformation is typical for any obstacle, but the greater the thickness of the barrier than stronger this effect becomes. It is important to note that the front of the wave in this case approaches the x coordinate in 16 m at time $t \approx 21.5$ sec. The passage of the entire wave at this point ($x = 16$ m) takes about 13 sec. At time $t \approx 28$ sec there is a redistribution of the velocity between the flow and the vortices. The wave speed begins to decay, while the vortex structures become pronounced. At time $t \approx 31$ sec six well-formed vortices are visible. In comparison with the case for a short obstacle (Fig. 8), the most intense vortices are formed very far from the obstacle, while for the case $D = 0.01$ m the strongest vortex flow appears directly behind the obstacle. This effect is observing with increasing thickness D.

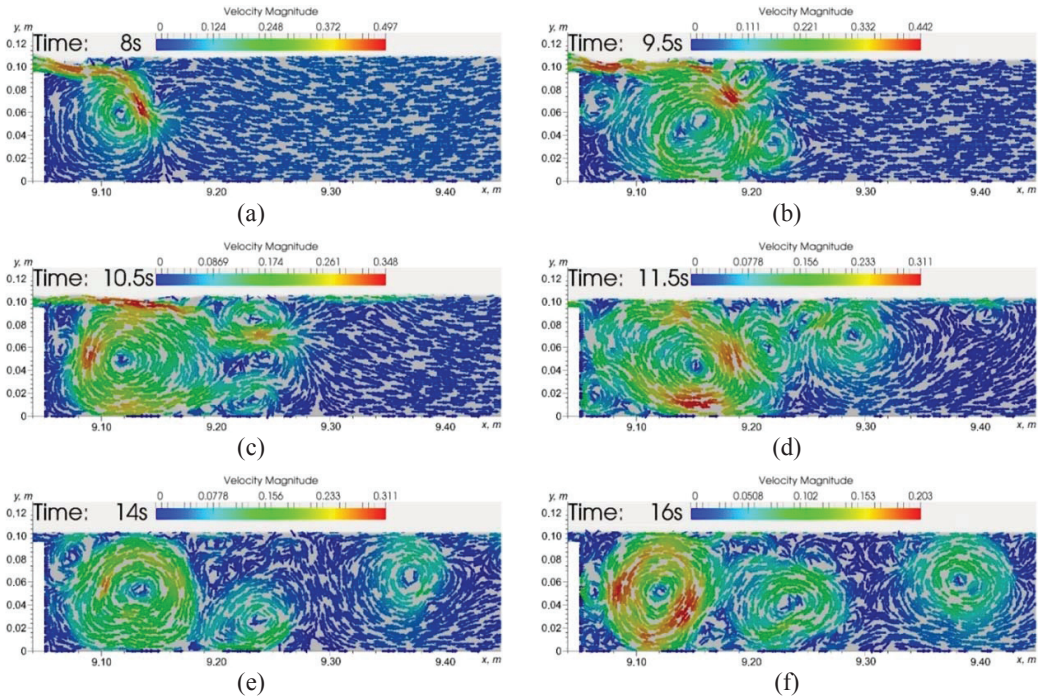

FIGURE 7. Vortex field evolution behind the obstacle at $H = 0.103$ m, $A = 0.007$ m, $D = 0.01$ m.

The thickness of barrier D strongly affects to the character of vortex formation. Noted that while $D < \lambda$ the character of the vortex formation is very similar to the case for a thin barrier. The number of strong vortices usually does not exceed three and them forming immediately behind the barrier. Once $D < \lambda$ the flow behind the barrier become similar to the case described in Fig. 8.

Wave Transmission and Reflection Coefficients

The results of calculations of the relative reflection energies (Wr), relative transmission energies (Wt) and the sums of these energies with respect to the incident wave total energy $(Wr + Wt)/W$ are shown in Fig. 9. Figure 9 shows the thickness of the obstacle D in dimensionless form with respect to the wavelength λ. The graph clearly shows that the greater thickness of the barrier relative to the wavelength, that the stronger decreases the energy of the wave. The energy of the reflected wave (Wr) at a value of $D/\lambda \geq 0.125$ remains constant and an increase

the thickness of the obstacle has no effect. The energy of the transmitted wave for small D/λ varies wavelike, but even for $D/\lambda \geq 0.250$ it decreases linearly. The sum of the energies $Wr + Wt$ with respect to the total wave energy increases for small D/λ, but then it starts to decrease linearly.

From Fig. 9 it can be said that the incident wave falling on the obstacle fades out more if the thickness of the obstacle with respect to the wavelength increases. The energy decrease at $D/\lambda \geq 0.250$ occurs linearly and, therefore, can be predict with great accuracy. Energy minimum is reaching at the maximum possible length of the barrier.

Consequently, most of the wave energy remains in the vortex structures formed above the barrier and behind it. Fig. 9 shows that 40-60% of the energy of the incident wave is retain in the vortices.

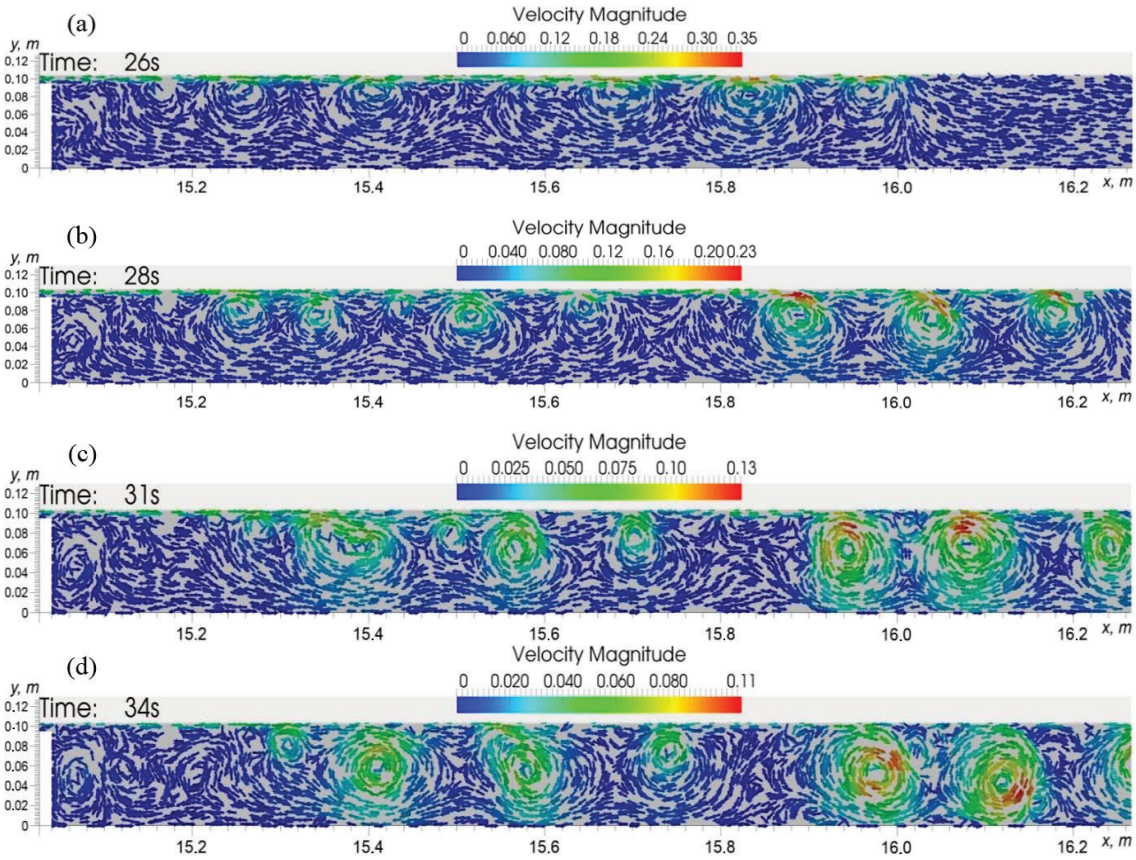

FIGURE 8. Vortex field evolution behind the obstacle at $H = 0.103$ m, $A = 0.007$ m, $D = 6$ m

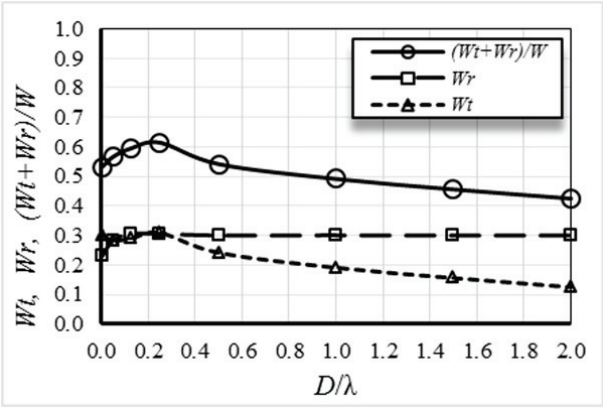

FIGURE 9. Relative reflection energies (Wr), relative transmission energies (Wt) and the sums of these energies with respect to the incident wave total energy $(Wt + Wr)/W$ depending on the thickness of the obstacle D/λ

CONCLUSION

In this study, a detailed analysis in a viscous formulation of a long hydrodynamic tsunami-like wave interaction with submerge impermeable barriers of different thicknesses is carried out. The process of wave generation, wave propagation through a channel, interaction with an obstacle, passing of a wave over a barrier and processes of vortex formation has been discussed in this work. The following summarizes the major findings and conclusions of this study.

(1) Comparison with experiment, by drawing an oscillogram of the free surface displacement, shows a fairly accurate justification of numerical calculations and experimental data. The wave arrival time on the sensors and the height of the free surface displacement, make it possible to estimate the velocities and energies of the waves using the integral method.

(2) A number of features characterize the wave interaction with an obstacle of different thickness. Thin obstacles at $D << \lambda$ cannot significantly slow down the wave. The wave flows through the barrier and forms strong vortices immediately behind the obstacle, and the number of vortices does not exceed three. Increasing the thickness of the barrier increases the wavelength. When a wave hits an obstacle with a thickness $D \geq \lambda$, small vorticity forming on the surface of the barrier due to interaction with the straight ledge, which causes to decelerate the flow. Behind a thick barrier in the case when $D \geq \lambda$, the intensity of the forming vortex structures is lower than in the case of thin barriers, but a greater number of vortex structures are formed.

The integral estimation of the incident, reflected and transmitted waves was showed that an increase the thickness of the submerge dike could leads to a weakening of the transmitted wave. The transmitted wave energy decrease has a linear dependence. An estimate of the sums of relative energies makes it possible to say that the vortex structures formed by the wave interaction with the obstacle take on them are above 40 to 60% of the incident wave energy.

This information will allow the future creation of effective structures to combat the destructive energy of tsunamis.

ACKNOWLEDGEMENTS

This work was supported by grant No.15-08-04097a of the Russian Foundation for Basic Research.

REFERENCES

1. B.V. Levin and M.A. Nosov, *Physics of tsunami and related phenomena in the ocean* (Moscow, Yanus K, Russia, 2005), p.360 (in Russian).
2. M.A. Losada, C. Vidal and R. Medina, J. Geophys. Res. **94**, 557–566 (1989).
3. A.M. Fridman, L.S. Alperovich, L. Shemer, L.A. Pustilnik, D. Shtivelman, An.G. Marchuk and D. Liberzon, *Physics-Uspekhi*. **180(8)**, 843–850 (2010).
4. E. Irtem, E. Seyfioglu and S. Kabdasli, J. Coast. Res., SI **64**, 516–520 (2011).
5. Y. Saprykina, S. Kuznetsov and D. Korzinin, Procedia Eng. **116**, 187–194 (2015).
6. V. Sriram, I. Didenkulova, A. Sergeeva and S. Schimmels, Coastal Eng. **111**, 1–12 (2016).
7. B.V. Boshenyatov, [Features of modeling tsunami waves in a laboratory installation]. Proceedings of the XIX Anniversary International Conference CMMAAS'2015. Alushta, Crimea, 2015. pp. 384–385 (in Russian).
8. B.V. Boshenyatov, Y.K. Levin, V.V. Popov and A.V. Semyanistyi, Instrum. Exp. Tech. **54(2)**, 254–255 (2011).
9. B.V. Boshenyatov, Y.K. Levin and V.V. Popov, RF Patent 2485452 (20 June 2013).
10. L. Daming and L. Yangyang, Acta Oceanol. Sin. **34(5)**, 103–109 (2015).
11. E.I. Borzenko and G.R. Shrager, J. Eng. Phys. Thermophys. **89(4)**, 902–910 (2016).
12. V.A. Arkhipov, S.S. Bondarchuk, A.S. Usanina and G. R. Shrager, J. Eng. Phys. Thermophys. **88(1)**, 42–51, (2015).
13. A.V. Shvab and N.S. Evseev, Theor. Found. Chem. Eng. **49(2)**, 191–199 (2015).
14. I. Wijatmiko and K. Murakami, J. Hydrodyn. **22(5)**, 259–264 (2010).
15. M. D. Jesus, J. L. Lara and I. J. Losada, J. App. Mathem. **V.2012**, 1–27 (2012).
16. Y.-T. Wu, S.-C. Hsiao, Z.-C. Huang and K.-S. Hwang, Coastal Eng. **62**, 31–47 (2012).
17. C.-J. Huang and C.-M. Dong, Coastal Eng. **43**, 265–286 (2001).
18. M. Sarfaraz and A. Pak, Coastal Eng. **121**, 145–157 (2017).
19. K. Qu, X.Y. Ren and S. Kraatz, Applied Ocean Research **63**, 36–48 (2017).
20. C. Jiang, X. Liu, Y. Yao, B. Deng and J. Chen, J. Earthq. Tsunami **11(1)**, 18 (2016).

21. B. Boshenyatov and D. Lisin, "Modeling of Tsunami Waves in an Open Hydrodynamic Channel," in *Proc. of the 8th Int. Symp. on Advanced Science and Technology in Experimental Mechanics.* Report **123**, Sendai, Japan (2013).
22. B.V. Boshenyatov, Doclady Physics. **58(10)**, 453–456 (2013).
23. B.V. Boshenyatov and K.N. Zhiltsov, AIP Conf. Proc. **1770**, 030088 (2016).
24. C.W. Hirt and B.D. Nichols, J. Comput. Phys. **39**, 201–225 (1981).
25. S.S. Kutateladze, B.P. Mironov, V.E. Nakoryakov and E.M. Khabakhpasheva, *Experimental Investigations Near-wall Turbulent Flows* (Novosibirsk, Science SD, 1975), p. 166 (in Russian).
26. S.V. Patankar, *Numerical Heat Transfer and Fluid Flow* (CRC Press. 1980). 312 p.
27. OpenFOAM Foundation. OpenFOAM. User guide. Available at http://www.openfoam.org, 211 p. (2016).
28. B.V. Boshenyatov and K.N. Zhiltsov, Modern High Technol. **12-1,** 20–23 (2015).